Separation Science and Technology
Publication details, including instructions for authors and subscription information:
http://www.informaworld.com/smpp/title~content=t713708471

Adsorption of Off-Gases from Steam Methane Reforming (H_2, CO_2, CH_4, CO and N_2) on Activated Carbon

Carlos A. Grande[a]; Filipe V. S. Lopes[a]; Ana M. Ribeiro[a]; José M. Loureiro[a]; Alírio E. Rodrigues[a]
[a] Faculty of Engineering, Laboratory of Separation and Reaction Engineering (LSRE), Associate Laboratory, Department of Chemical Engineering, University of Porto, Porto, Portugal

To cite this Article Grande, Carlos A. , Lopes, Filipe V. S. , Ribeiro, Ana M. , Loureiro, José M. and Rodrigues, Alírio E.(2008) 'Adsorption of Off-Gases from Steam Methane Reforming (H_2, CO_2, CH_4, CO and N_2) on Activated Carbon', Separation Science and Technology, 43: 6, 1338 — 1364
To link to this Article: DOI: 10.1080/01496390801940952
URL: http://dx.doi.org/10.1080/01496390801940952

Separation Science and Technology, 43: 1338–1364, 2008

ISSN 0149-6395 print/1520-5754 online
DOI: 10.1080/01496390801940952

Adsorption of Off-Gases from Steam Methane Reforming (H_2, CO_2, CH_4, CO and N_2) on Activated Carbon

Carlos A. Grande, Filipe V. S. Lopes, Ana M. Ribeiro, José M. Loureiro, and Alírio E. Rodrigues

Faculty of Engineering, Laboratory of Separation and Reaction Engineering (LSRE), Associate Laboratory, Department of Chemical Engineering, University of Porto, Porto, Portugal

Abstract: Hydrogen is the energy carrier of the future and could be employed in stationary sources for energy production. Commercial sources of hydrogen are actually operating employing the steam reforming of hydrocarbons, normally methane. Separation of hydrogen from other gases is performed by Pressure Swing Adsorption (PSA) units where recovery of high-purity hydrogen does not exceed 80%.

In this work we report adsorption equilibrium and kinetics of five pure gases present in off-gases from steam reforming of methane for hydrogen production (H_2, CO_2, CH_4, CO and N_2). Adsorption equilibrium data were collected in activated carbon at 303, 323, and 343 K between 0-22 bar and was fitted to a Virial isotherm model. Carbon dioxide is the most adsorbed gas followed by methane, carbon monoxide, nitrogen, and hydrogen. This adsorbent is suitable for selective removal of CO_2 and CH_4. Diffusion of all the gases studied was controlled by micropore resistances. Binary (H_2-CO_2) and ternary (H_2-CO_2-CH_4) breakthrough curves are also reported to describe the behavior of the mixtures in a fixed-bed column. With the data reported it is possible to completely design a PSA unit for hydrogen purification from steam reforming natural gas in a wide range of pressures.

Keywords: Hydrogen, carbon dioxide, pressure swing adsorption, adsorption equilibrium, multicomponent breakthrough curves

Received 26 June 2007, Accepted 27 December 2007

Address correspondence to Alírio E. Rodrigues, Faculty of Engineering, Laboratory of Separation and Reaction Engineering (LSRE), Associate Laboratory, Department of Chemical Engineering, University of Porto, Porto, Portugal. Tel.: + 351 22 508 1671; Fax: +351 22 508 1674; E-mail: arodrig@fe.up.pt

INTRODUCTION

To avoid unknown consequences in global weather, there is a general consensus that the emission of anthropogenic greenhouse gases to atmosphere should be reduced significantly. This environmental pressure is translated to economic penalties to countries included in the Annex B of the Kyoto protocol. One of the alternatives to reduce GHG emissions is to capture CO_2 in the source, namely power plants. The carbon capture process is strongly dependent on the power station technology. Actually, three different technologies for power generation are being considered (1): post-combustion, pre-combustion, and oxyfuel. The CO_2 captured should then be permanently sequestered (2).

The pre-combustion process for capture of CO_2 consists of a separation technique located after a partial combustion of fossil fuels for production of hydrogen. The important goal in this process is a carbon dioxide capture technique from steam methane reformers (SMR) off-gas. Production of hydrogen in centralized units will allow a transition phase where fossil-fuels can be employed for its generation and the produced CO_2 can be locally concentrated for permanent sequestration. Another interesting application of hydrogen is in mobile sources, replacing fossil-fuels where its combustion release water instead of other greenhouse gases that are actually responsible for climate change. If the process to obtain hydrogen is also able to concentrate the CO_2 formed, storage or other alternatives may be employed to avoid its emissions to atmosphere reducing the impact of the process to the environment. The development of such a process is the main task of the European Research Project HY2SEPS (Hybrid Hydrogen Carbon Dioxide Separation Processes), where Pressure Swing Adsorption (PSA) technology is combined with a membrane process to achieve this goal (3).

The current technology to separate hydrogen from other gases coming from SMR off-gas is PSA (4–9). The gases involved in the PSA unit are: hydrogen, carbon dioxide, carbon monoxide, methane and water. If the methane employed in the reforming contains nitrogen, this gas will also be present in the separation. The PSA unit normally consists of a multi-column set up of adsorbers (10): an initial layer removes water, carbon dioxide and methane while a second layer of a zeolite removes other components until reaching less than 10 ppm of CO in the product. To increase the hydrogen recovery, complex scheduling of the columns is required and normally more than eight columns are employed. There is a great pressure to increase hydrogen recovery and reduce the unit capital cost, indicating that research in both new materials and in the separation process is required. Moreover, the CO_2-rich stream obtained cannot be used for sequestration since it contains significant amounts of H_2 and CH_4, that in addition to the required special handling, have also significant value as fuels.

In this work we study the fundamental properties of the different gases and in multicomponent mixtures in a commercial sample of activated carbon to be employed in PSA units to remove contaminants from SMR off-gas, namely CO_2, CH_4, and CO. We have measured adsorption equilibrium and kinetics of all the gases comprising the off-gas SMR mixture in dry basis: hydrogen, carbon dioxide, methane, carbon monoxide and nitrogen. Note that the data presented in this work has no water, thus this component should be removed in a previous step to avoid preferential adsorption in the adsorbent. The conditions of the measurements comprise temperature range between 303–343 K and a wide range of pressures covering 0–22 bar for the main components (H_2 and CO_2). Binary breakthrough experiments of H_2/CO_2 mixtures and ternary breakthrough experiments of $H_2/CO_2/CH_4$ mixtures are also presented. The adsorption equilibrium data was analyzed employing a Virial isotherm that describes the behavior of the multicomponent mixture based on the parameters fitted to pure component data.

EXPERIMENTAL

Adsorption Equilibrium

Adsorption equilibrium of pure gases (H_2, CO_2, CH_4, CO, and N_2) was measured in a magnetic suspension microbalance (Rubotherm, Germany) operated in closed system. Two Lucas Schaevitz pressure transducers were used to measure the pressure inside the adsorption chamber: one from 0–1 bar and other from 0–250 bar to acquire data with good accuracy at low and high-pressures, respectively. The activation of the activated carbon sample was carried out under vacuum ($<10^{-7}$ bar) at 423 K overnight. The heating rate to reach this temperature was 1 K/min.

Adsorption equilibrium isotherms were measured at 303, 323, and 343 K. Adsorption and desorption measurements were performed and all the isotherms reported were reversible. The value obtained from experimental adsorption measurements corresponds to the excess adsorbed phase concentration. Correction of buoyancy has been taken into account to report the absolute amount adsorbed. The buoyancy effect becomes important when pressure increases, i.e. when the gas density becomes closer to the density of the adsorbed phase (11). As the density of the adsorbed phase cannot be measured directly, the absolute amount adsorbed cannot be obtained experimentally and many approximate methods to calculate it from the excess adsorption were published (11–13). In order to take into account the effects of buoyancy in all the experimental data measured in this work, we have employed the assumption that the density of the adsorbed phase is approximated with the density of the liquid at its boiling point at 1 atm (13). Employing this equation, the correction of the buoyancy was performed

according to the following Equation (14):

$$q = \frac{\Delta m + \rho_g(V_s + V_c)}{m_s M_W} \frac{\rho_\ell}{\rho_\ell - \rho_g} \tag{1}$$

where q is absolute adsorbed phase concentration, (Δm) is the difference of weight between one measurement and the previous one, ρ_g is the density of the gas phase, ρ_ℓ is the density of the adsorbed phase, V_s is the volume of the solid adsorbent and V_c is the volume of the cell where the adsorbent is located, m_s is the mass of adsorbent connected to the microbalance and M_W is the molecular weight of the gas. In order to determine the volumes that contribute to the buoyancy effect ($V_s + V_c$), a calibration with helium was performed, under the assumption that this gas is not adsorbed ($m_{ads} = V_{ads} = 0$). A constant value for liquid phase density (boiling point at 1 atm of pressure), was employed for all the temperatures studied (13, 15, 16). Measurements of carbon monoxide were performed only at low partial pressures and we have assumed that the buoyancy corrections are negligible.

Adsorption Kinetics

Adsorption kinetics of pure gases was measured employing two different techniques. For carbon dioxide we used diluted breakthrough curves: employing a very small concentration of CO_2 in a diluted stream of an inert gas (helium) we can assume that the isotherm is linear, velocity is constant and also that the column is at the same temperature (isothermal behaviour). For the case of hydrogen, carbon monoxide, and methane, we measured the response to a pulse of these gases. Diluted concentrations of these gases were used to measure the diffusivities in the linear region of the isotherm. By determining the first moment (stoichiometric time) and the second moment, both equilibrium and kinetic properties can be determined. The apparatus employed for these measurements is composed of a column where the adsorbent is loaded and a four-way valve where two streams are inlet streams: one with the diluted stream with CO_2 and the other with inert gas for desorption. In the case of pulse experiments, the gas is injected into the inert gas stream in the injector very close to the column with a gas-tight syringe. The operating conditions and physical properties of both systems are reported in Table 1. Note that the column for H_2 has to be larger to have reliable data of adsorption kinetics since H_2 is a gas with little adsorption capacity at low partial pressures and very fast kinetics.

Multicomponent Breakthrough Curves

In order to verify the adsorption equilibrium obtained by gravimetry and the adsorption kinetics of pure components, multicomponent binary H_2/CO_2

Table 1. Experimental conditions used on the measurement of the CO_2 diluted breakthroughs and of the CH_4, CO and H_2 pulses

Experiments	Diluted breakthrough	Pulse experiments	
Adsorbate (Ads)	CO_2	CH_4 and CO	H_2
Mixtures	0.5% of Ads in He	—	—
Inert gas	He	He	He
Mass of Adsorbent [kg]	5.0324×10^{-3}	5.0324×10^{-3}	1.116×10^{-1}
Temperatures [K]	303, 323, 343	303, 323, 343	303
Pressure [bar]	1	1	1
Bed height [m]	0.167	0.167	0.254
Bed volume [m^3]	9.476×10^{-6}	9.476×10^{-6}	2.005×10^{-4}
Pellet porosity, ε_p	0.601	0.601	0.601
Adsorbent density, ρ_p [kg/m^3]	841	841	841
Solid density, ρ_s [kg/m^3]	2110	2110	2110
Bed porosity, ε	0.392	0.392	0.363

and ternary $H_2/CO_2/CH_4$ breakthrough experiments were performed in a fixed bed. Activation of the adsorbent was carried out at 423 K (heating rate of 1 K/min) overnight under flow of helium. Carbon dioxide and methane concentrations exiting the column were measured by an infrared detector each ten seconds (flue gas analyzer, Madur, Austria). In the binary mixture, ethane was inserted as a tracer gas to determine flowrate variations. The flowrate variations were determined with a flow sensor FLR1006 (Omega, USA). The temperature in the column was measured at three points: at 0.17, 0.43, and 0.68 m from the feed inlet.

THEORETICAL

Adsorption Equilibrium

From the large number of mathematical models available in literature to describe adsorption equilibria (17), we have selected the Virial equation (18, 19). This model is thermodynamically correct at low and high coverages, has analytical expressions for prediction of multicomponent behavior, and also is very flexible to fit isotherms with different degrees of steepness in a wide range of pressure and temperature conditions. The model is obtained by applying the bi-dimensional Virial equation of state to the Gibbs isotherm that results in:

$$P = \frac{q}{K_H}\exp\left(\frac{2}{S}Aq + \frac{3}{2S^2}Bq^2 + \ldots\right) \tag{2}$$

In this equation, S is the adsorbent specific surface area, A and B are Virial coefficients, and K_H is the Henry constant. The Henry constant is related to the temperature (T) through the Van't Hoff equation:

$$K_H = K_\infty \exp\left(\frac{-\Delta H}{R_g T}\right) \tag{3}$$

where K_∞ is the adsorption constant at infinite temperature, $(-\Delta H)$ is the heat of adsorption at zero coverage and R_g is the universal gas constant.

For most systems the Virial equation can be truncated after the second Virial coefficient and the coefficients depend on the temperature through the following equations:

$$A = \sum_{m=0}^{\infty} \frac{A_m}{T^m}, \quad B = \sum_{m=0}^{\infty} \frac{B_m}{T^m} \tag{4}$$

Taqvi and LeVan (20) extended the Virial isotherm to multicomponent adsorption in a predictive mode as follows:

$$P_i = \frac{q_i}{K_{Hi}} \exp\left(\frac{2}{S}\sum_{j=1}^{N} A_{ij} q_j + \frac{3}{2S^2}\sum_{j=1}^{N}\sum_{k=1}^{N} B_{ijk}\, q_j q_k\right) \tag{5}$$

with the mixing Virial coefficients (A_{ij} and B_{ijk}) calculated by (21):

$$A_{ij} = \frac{(A_i + A_j)}{2} \tag{6}$$

$$B_{ijk} = \frac{(B_i + B_j + B_k)}{3} \tag{7}$$

The parameters obtained from the fitting of pure gases can be employed in the prediction of multicomponent adsorption equilibrium to design a PSA unit. The multi-parametric nonlinear fitting was performed using MATLAB (The MathWorks, Inc.). The minimization routine uses the Nelder – Mead Simplex Method of direct search (*fmins*). The error function defined was:

$$ERR(\%) = 100\left[w \sum_T \sum_P (q_{cal} - q_{exp})^2 + \frac{(1-w)}{N} \sum_T \sum_P \left(\frac{q_{cal} - q_{exp}}{q_{cal}}\right)^2 \right] \tag{8}$$

where T is each experimental temperature, P is the pressure, N is the number of points of each isotherm, q_{exp} is the experimental adsorbed phase concentration, and q_{cal} is the calculated adsorbed phase concentration. The term w is the weight *SOR-ARE* parameter ($0 \le w \le 1$). This error function is composed by two terms defined as Square of Residuals (22) and Average of residuals (17).

Adsorption Kinetics

The analyses of the pulse experiments (CH_4, CO, and H_2) and of the diluted breakthrough curves (CO_2) were performed with the analysis of the moments (23) where the first and second moments are calculated from the experimental data by:

$$\mu_1 \equiv \frac{\int_0^\infty t.c.dt}{\int_0^\infty c.dt} \tag{9}$$

$$\sigma^2 = \frac{\int_0^\infty (t-\mu_1)^2 \cdot c.dt}{\int_0^\infty c.dt} \tag{10}$$

The second moment analysis of a pulse or of a diluted breakthrough curve can be related with the sum of all diffusional resistances by (Ruthven, 1984):

$$\frac{\sigma^2}{2\mu_1^2} = \frac{D_{ax}}{u_i L} + \left(\frac{u_i}{L}\right)\left(\frac{\varepsilon}{1-\varepsilon}\right)\left(\frac{R_p}{2k_f} + \frac{R_p^2}{8\varepsilon_p D_p} + \frac{r_c^2}{8K_H D_c}\right) \times \left(1 + \frac{\varepsilon_p}{(1-\varepsilon_p)K_H}\right)^{-2} \tag{11}$$

where the axial dispersion and the film mass transfer coefficients were calculated according to the following equations:

$$D_{ax} = (0.45 + 0.55\varepsilon)D_m + 0.35R_p u_i \tag{12}$$

$$Sh = 2.0 + 1.1Re^{0.6}Sc^{1/3} \tag{13}$$

where $Sh(=2R_p k_f/D_m)$ is the Sherwood number and k_f is the film mass transfer coefficient, $Re(=2\rho_g u_o R_p/\mu)$ is the Reynolds number and $Sc(=\mu/\rho_g D_m)$ is the Schmidt number.

The pore diffusivity was calculated with the Bosanquet equation:

$$\frac{1}{D_{p,i}} = \tau_p\left(\frac{1}{D_{m,i}} + \frac{1}{D_{k,i}}\right) \tag{14}$$

where $D_{m,i}$ is the molecular diffusivity, $D_{k,i}$ is Knudsen diffusivity, both for component i, and τ_p is the pore tortuosity. The molecular diffusivity for the mixture was approximated with:

$$D_{m,i} = \frac{1-y_i}{\sum_{\substack{j=1 \\ j\neq i}}^{n} (y_i/D_{ij})} \tag{15}$$

where the binary molecular diffusivity D_{ij} was calculated with the Chapman-Enskog Equation (24). The Knudsen diffusivity ($D_{k,i}$ in m^2/s) is calculated by:

$$D_{k,i} = 0.97 r_p \sqrt{\frac{T_g}{M_W}} \tag{16}$$

where r_p is the mean pore radius (m) and M_W is the molecular weight of the adsorbate.

The micropore diffusion is an activated process with exponential dependence with temperature according to:

$$\frac{D_c}{r_c^2} = \frac{D_c^0}{r_c^2} \exp\left(-\frac{E_a}{R_g T}\right) \tag{17}$$

where D_c^0/r_c^2 is the limiting diffusivity (divided by r_c^2) at infinite temperature and E_a is the activation energy.

Multicomponent Breakthrough Curves

A complete mathematical model that describes the dynamic behavior of multicomponent adsorption in a fixed bed is composed of material, momentum and energy balances. The energy balance should be taken into account because adsorption is an exothermic process that releases energy and may produce non isothermal behaviour of the system. The momentum balance should also be included as the velocity varies along the bed.

The following assumptions were made in order to write the necessary conservation equations:

1. Ideal gas behaviour throughout the column, (operation up to 7 bar),
2. No mass, heat or velocity gradients in the radial direction,
3. Axial dispersed plug flow,
4. External mass and heat transfer resistances expressed with the film model,
5. Bidispersed adsorbent particle with macropore and micropore mass transfer resistances, both expressed with the Linear Driving Force (LDF) model,
6. No temperature gradients inside each particle,
7. Constant porosity along the bed.

A schematic diagram of this adsorption system is shown in Fig. 1 where three phases can be distinguished: gas phase, solid phase where adsorption and diffusion take place and the column wall where energy may be transferred to (or from) the surroundings.

The gas phase exchanges mass and energy with the solid phase and only energy with the column wall. The material balance for each component in the

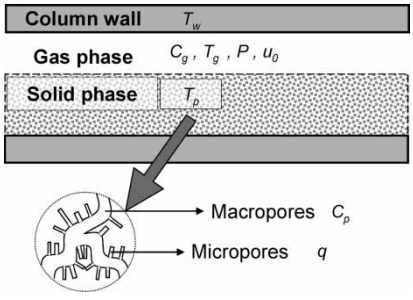

Figure 1. Schematic representation of the adsorption bed.

gas phase is given by:

$$\frac{\partial}{\partial z}\left(\varepsilon D_{ax} C_{g,T} \frac{\partial y_i}{\partial z}\right) - \frac{\partial}{\partial z}(u_0 C_{g,i}) - \varepsilon \frac{\partial C_{g,i}}{\partial t} - (1-\varepsilon) a_p k_f (C_{g,i} - C_{s,i}) = 0 \tag{18}$$

where z is the axial position, t is the time, ε is the bed porosity, u_0 is the superficial velocity, $C_{g,T}$ and $C_{g,i}$ are respectively the total and component i gas phase concentration, y_i is the component i molar fraction, $C_{s,i}$ is the concentration of component i at the solid surface, D_{ax} is the mass axial dispersion coefficient, k_f is the film mass transfer coefficient and a_p is the particle specific area.

In the momentum balance we have only considered the terms of pressure drop and velocity change and are related through the Ergun equation defined as:

$$-\frac{\partial P}{\partial z} = \frac{150\mu(1-\varepsilon)^2}{\varepsilon^3 d_p^2} u_0 + \frac{1.75(1-\varepsilon)\rho_g}{\varepsilon^3 d_p} |u_0| u_0 \tag{19}$$

where P is the total pressure, μ is the gas viscosity, ρ_g is the gas density, and d_p is the particle diameter.

The energy balance in the gas phase is:

$$\frac{\partial}{\partial z}\left(\lambda \frac{\partial T_g}{\partial z}\right) - u_0 C_{g,T} C_p \frac{\partial T_g}{\partial z} + \varepsilon R_g T_g \frac{\partial C_{g,T}}{\partial t} - (1-\varepsilon) a_p h_f (T_g - T_p) - \frac{4h_w}{d_{wi}}(T_g - T_w) - \varepsilon C_{g,T} C_v \frac{\partial T_g}{\partial t} = 0 \tag{20}$$

with T_g, T_p, and T_w respectively as the gas, particle and wall temperatures; C_v and C_p as the gas molar specific heat at constant volume and pressure respectively; R_g as the ideal gas constant; d_{wi} as the wall internal diameter, λ as the heat axial dispersion coefficient. The film heat transfer coefficient between the gas phase and the particle is represented by h_f, while the film heat transfer coefficient between the gas phase and the wall is represented by h_w.

As mentioned above, the particle is considered bidisperse, composed by macropores that serve as main transport channels to the micropores (Fig. 1). The macropores exchange mass both with the gas phase and the micropores. The linear driving force model (LDF) is employed to describe the mass transfer rates in the solid phase. This approximation has a large impact on the computational time. The material balances in the macropores and in the micropores are then given respectively by Equations (21) and (22).

$$\frac{\partial \overline{C_{m,i}}}{\partial t} = \frac{\Omega_m D_{p,i}}{R_p^2}(C_{s,i} - \overline{C_{m,i}}) - \frac{\rho_p}{\varepsilon_p}\frac{\partial \overline{q_i}}{\partial t} \tag{21}$$

$$\frac{\partial \overline{q_i}}{\partial t} = \frac{\Omega_c D_{c,i}}{r_c^2}(q_i^* - \overline{q_i}) \tag{22}$$

In these equations, ρ_p and ε_p are respectively the particle density and porosity, $D_{p,i}$ and $D_{c,i}$ are the macropore and micropore diffusivity coefficients, R_p is the particle radius, r_c is the "microparticle" radius, $\overline{C_{m,i}}$ is the averaged concentration in the macropores, $\overline{q_i}$ is the particle averaged adsorbed concentration, and q_i^* is the adsorbed concentration in equilibrium with $\overline{C_{m,i}}$ and Ω_c are the geometric LDF factors for the macro and micro particles respectively.

As it is assumed that there are no temperature gradients inside a particle, the solid phase energy balance is given by:

$$(1-\varepsilon)\left[\varepsilon_p \sum_{i=1}^{n} \overline{C_{m,i}} C_{v,i} + \rho_p \sum_{i=1}^{n} \overline{q_i} C_{v,ads,i} + \rho_p \hat{C}_{p,s}\right]\frac{\partial T_p}{\partial t}$$
$$= (1-\varepsilon)\varepsilon_p R_g T_p \frac{\partial \overline{C_{m,T}}}{\partial t} + \rho_b \sum_{i=1}^{n} (-\Delta H)_i \frac{\partial \overline{q_i}}{\partial t} + (1-\varepsilon) a_p h_f (T_g - T_p) \tag{23}$$

where ρ_b is the bulk density of the bed, $\hat{C}_{p,s}$ is the solid specific heat per mass unit and $(-\Delta H)_i$ is the isosteric heat of adsorption of component i.

The concentration of each component at the solid surface can be calculated with Equation (24) obtained through the fluxes equality at the particle surface.

$$C_{s,i} = \frac{Bi_i C_{g,i} + \overline{C_{m,i}}}{1 + Bi_i} \tag{24}$$

In this equation Bi_i is the Biot number of component i defined as:

$$Bi_i = \frac{a_p k_f R_p^2}{\varepsilon_p \Omega_m D_{p,i}} \tag{25}$$

Finally, the energy balance to the column wall considers that it interchanges energy with the gas phase inside the column and with the external environment being expressed as:

$$\rho_w \hat{C}_{p,w} \frac{\partial T_w}{\partial t} = \alpha_w h_w (T_g - T_w) - \alpha_{w\ell} U (T_w - T_\infty) \tag{26}$$

where T_∞ is the external temperature, ρ_w is the wall density, $\hat{C}_{p,w}$ is the wall specific heat per mass unit, U is the overall heat transfer coefficient, and α_w and $\alpha_{w\ell}$ are defined by:

$$\alpha_w = \frac{d_{wi}}{e(d_{wi} + e)}; \quad \alpha_{w\ell} = \frac{1}{(d_{wi} + e)\ln(d_{wi} + e/d_{wi})} \tag{27}$$

where e is the wall thickness.

In order to solve this system of partial differential equations, boundary and initial conditions are needed. In the case of fixed bed operation where pressure is controlled at the end of the column, starting with a column filled with an inert gas, such conditions are as follows:

Feed inlet ($z = 0$)

$$u_{0inlet} C_{inlet,i} = u_0 C_{g,i} - \varepsilon D_{ax} C_{g,T} \frac{\partial y_i}{\partial z} \tag{28}$$

$$u_{0inlet} C_{inlet,T} = u_0 C_{g,T} \tag{29}$$

$$u_{0inlet} C_{inlet,T} C_p T_{inlet} = u_0 C_{g,T} C_p T_g - \lambda \frac{\partial T_g}{\partial z} \tag{30}$$

Product end ($z = L$)

$$\frac{\partial C_{g,i}}{\partial z} = 0 \tag{31}$$

$$P = P_{exit} \tag{32}$$

$$\frac{\partial T_g}{\partial z} = 0 \tag{33}$$

The initial conditions for the fixed bed initially filled with inert gas are:

$$y_i = \overline{C_{m,i}} = q_i = 0 \quad for\ i \neq inert \tag{34}$$

$$y_{inert} = 1 \tag{35}$$

$$\overline{C_{m,inert}} = C_{g,T} \tag{36}$$

$$T_g = T_p = T_w = T_{inlet} \tag{37}$$

As can be seen from the model equations, some transport parameters are needed. General properties of the gases, like density, viscosity, and thermal conductivity were calculated according to Bird et al. (24). The molecular diffusivity for the mixture and the Knudsen diffusivity were calculated according to Equations (14–16), respectively. The axial heat dispersion coefficient, as well as, the heat convective coefficient were calculated using the Wakao and Funazkri correlations (23, 25, 26):

$$\frac{\varepsilon D_{ax}}{D_m} = 20 + 0.5 Sc\, Re \tag{38}$$

$$\frac{\lambda}{k_g} = 7 + 0.5 Pr\, Re \tag{39}$$

$$Nu = 2.0 + 1.1 Re^{0.6} Pr_i^{1/3} \tag{40}$$

The axial mass transfer coefficient calculated by Equation (40) is valid for a large range of Reynolds numbers ($3 < \mathrm{Re} < 10{,}000$) and was employed for modeling multicomponent breakthrough curves reported in this work. The dimensional Nusselt number is defined as $Nu = h_f d_p / k_g$.

The global heat transfer coefficient, U, was calculated according to (27):

$$\frac{1}{U} = \frac{1}{h_w} + \frac{e d_{wi}}{\lambda_w d_{\ell n}} + \frac{d_{wi}}{d_{we} h_{ex}} \tag{41}$$

where λ_w is the wall conductivity, d_{we} is the external diameter of the column, $d_{\ell n} = (d_{we} - d_{wi})/\ln(d_{we}/d_{wi})$, and h_{ex} is the external convective heat transfer coefficient. The internal convective heat transfer coefficient h_w between gas and the wall column can be estimated with the Wasch and Froment correlation (28):

$$\frac{h_w d_{wi}}{k_g} = 140 + 0.013396 \frac{d_{wi}^2}{d_p k_g} Re \tag{42}$$

The external convective heat transfer coefficient was estimated with the Churchill and Chu correlation (27):

$$\frac{h_{ex} L}{k_{g,ex}} = 0.68 + \frac{0.67 Ra^{1/4}}{\left[1 + (0.492/\mathrm{Pr})^{9/16}\right]^{4/9}} \tag{43}$$

where the sub-index *ex* represent the properties of the external gas surrounding the column. The Rayleigh number is defined by: $Ra = Gr\mathrm{Pr}$ and the Grashof number is:

$$Gr = \frac{g\beta(T_w - T_\infty)L^3}{\nu\alpha} \tag{44}$$

where $g = 9.8\ \mathrm{m/s^2}$, ν is the kinematic viscosity of the external gas, α is the external thermal diffusivity, and β is the thermal expansion coefficient. The

properties of the external gas are evaluated at the film temperature: $T_{film} = (T_w + T_\infty)/2$.

This mathematical model has already been used in the simulation of fixed bed behaviour and Pressure Swing Adsorption (PSA) applications of different mixtures showing very good agreement between predictions and experimental data (29–31). The simulations were performed with *gPROMS* (PSE Enterprise, UK) using the orthogonal collocation on finite elements as the numerical method. The number of elements used was 120 with forth order polynomials (three interior collocation points).

RESULTS AND DISCUSSION

Adsorption Equilibrium

The fundamental property to be measured in a material that will be employed in an adsorption-based separation process is the adsorption equilibrium capacity of each of the pure gases employed. As explained in the Experimental section, the excess amount adsorbed is the amount measured experimentally and it had to be corrected to take into account the buoyancy effects. The absolute amount adsorbed of hydrogen and carbon dioxide at three different temperatures (303, 323 and 343 K) are shown in Fig. 2. The isotherms in the same temperature range for CH_4, CO and N_2 are reported in Fig. 3. Note that the pressure range measured for CO_2 and H_2 is much higher than for the other gases because these are the main components of the stream entering the PSA unit for H_2 purification. From these experiments we have observed the following order of adsorption (from the most adsorbed compound to the less adsorbed gas): $CO_2 > CH_4 > CO > N_2 > H_2$. It can be also observed that the isotherm of CO_2 is non-linear as well as the

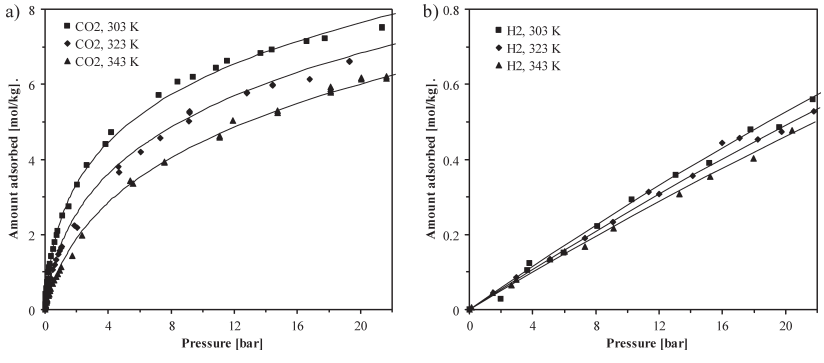

Figure 2. Amount of CO_2 (a) and H_2 (b) adsorbed on activated carbon: experimental points at 303 (■), 323 (◆) and 343 K (▲) and —— virial isotherm fitting.

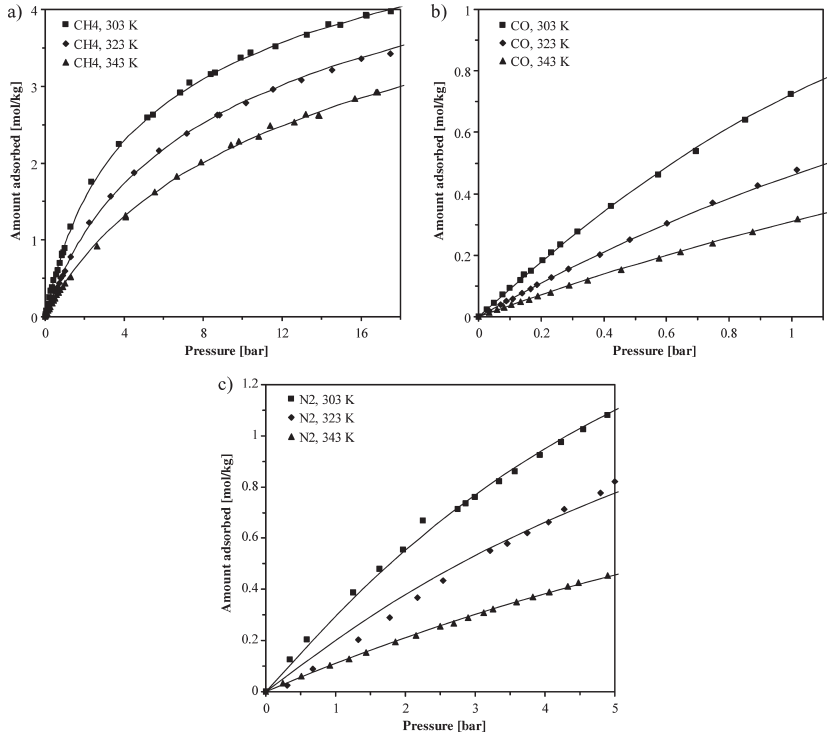

Figure 3. Amount of CH_4 (a), CO (b) and N_2 (c) adsorbed on activated carbon: experimental points at 303 (■), 323 (◆) and 343 K (▲) and —— virial isotherm fitting.

isotherm of CH_4, while the isotherms of other components are almost linear in the initial portion that corresponds to the concentration of the off-gas SMR streams.

The data obtained in this work for CO_2 and H_2 are comparable with other values reported in literature (32–34).

The experimental adsorption data were fitted using the Virial isotherm with the temperature dependence of the Virial coefficients truncated at the second term. The fitting of the model is shown with solid lines in Figs. 2 and 3. The parameters obtained for all the pure gases are presented in Table 2. It can be seen that a good fitting is obtained for all the gases in the whole pressure and temperature ranges studied. The Virial model showed great flexibility to fit the complete set of adsorption equilibrium data of the different gases with the additional advantage of direct prediction of multicomponent adsorption equilibrium, which is important to improve computation time of PSA process simulation. According to the fitting parameters, the heat of adsorption of CO_2 is much higher than the other gases, while CO heat of adsorption is slightly higher than the heat of adsorption of CH_4.

Table 2. Virial adsorption isotherm fitting parameters of CO_2, H_2, CH_4, CO and N_2 on activated carbon

Comp.	K_∞ [mol/(kg bar)]	$(-\Delta H)$ [J/mol]	$A_0 \times 10^{-5}$ [m^2/mol]	$A_1 \times 10^{-6}$ [m^2K/mol]	$B_0 \times 10^{-11}$ [m^4/mol^2]	$B_1 \times 10^{-11}$ [m^4K/mol^2]
CO_2	9.90×10^{-5}	27 870	−1.140	79.013	−0.021	−0.416
H_2	8.20×10^{-3}	3 192	0.418	−0.001	0.454	0.000
CH_4	1.04×10^{-3}	17 652	4.616	−121.43	−0.831	308.53
CO	4.62×10^{-4}	19 100	14.076	−422.77	0.264	299.25
N_2	2.54×10^{-3}	11 834	5.585	−163.77	3.385	−777.67

Adsorption Kinetics

Pressure Swing Adsorption is a dynamic separation process and thus it is important to measure the velocity of diffusion of the gases in the porous structure of the adsorbent. In several cases, the resistance to diffusion is so important that the PSA is kinetically controlled (35, 36). In this case, we have molecules of several sizes and chemical properties, reason why it is also very complicated to establish a common protocol, even to measure the diffusion process. Several techniques to measure the diffusion process are available: Zero Length Column (37), uptake curves (17, 23) and perturbation chromatography (either pulse or step changes). Activated carbons are porous solids with a somewhat wide distribution of micropore diameters. If ZLC experiments are performed in the samples and analyzed using the long time response, only the resistance in the smaller micropores will be accounted and then results of ZLC and breakthrough curves may give large differences (38). For this reason we have employed perturbation chromatography methods (39). Due to the hazardous nature of carbon monoxide we have employed only pulses. Also according to the higher sensitivity of Flame Ionization Detector (FID), we have employed very small amounts of CH_4 for pulse experiments. The diffusion of H_2 is extremely fast and its amount adsorbed is very small, reason why a much larger column was employed. Due to the non-linearity of CO_2 equilibrium isotherms and to plausible thermal effects associated with the large heat of adsorption, we have performed diluted breakthrough curves that ensure that concentrations of 0.5% are fed constantly to the column.

The experimental conditions used on the measurement of the carbon dioxide diluted breakthroughs and of the methane, carbon monoxide and hydrogen pulses are reported in Table 1. The results of the diluted breakthrough curves of carbon dioxide are shown in Fig. 4. Pulse experiments for both CH_4 and CO are shown in Fig. 5 and for H_2 in Fig. 6. It should be pointed out that the experimental error associated to the measurement of the peak of hydrogen is considerable because of the small difference of thermal

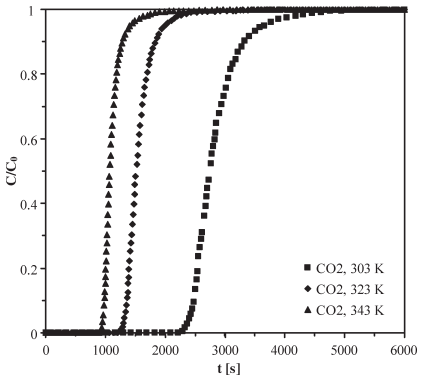

Figure 4. Diluted breakthrough curves of carbon dioxide on activated carbon at 303 (■), 323 (◆) and 343 K (▲); 1 bar of total pressure; experimental conditions are detailed in Table 2.

conductivities between helium (inert gas employed for pre-conditioning of the column) and hydrogen is small.

With the results obtained in this set of experiments, the first and second moments were calculated. The axial dispersion, film mass transfer coefficient and the macropore diffusivity are calculated from Equations (12–14). To estimate the pore diffusivity coefficient by the Bosanquet equation, a tortuosity factor of 2 was assumed for activated carbon.

The analyses of the diluted breakthrough curves on activated carbon obtained for carbon dioxide are shown in Table 3. The values obtained from the methane, carbon monoxide and hydrogen pulse experiments on activated carbon are shown in Tables 4 to 6, respectively.

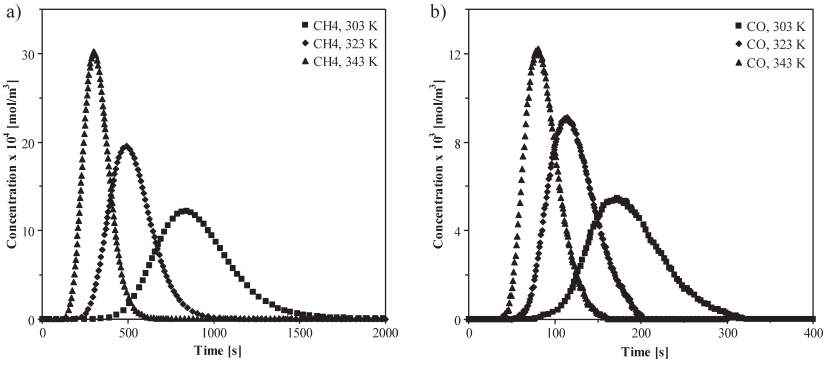

Figure 5. Pulse experiments of methane (a) and carbon monoxide (b) on activated carbon at 303 (■), 323 (◆) and 343 K (▲); 1 bar of total pressure; experimental conditions are detailed in Table 2.

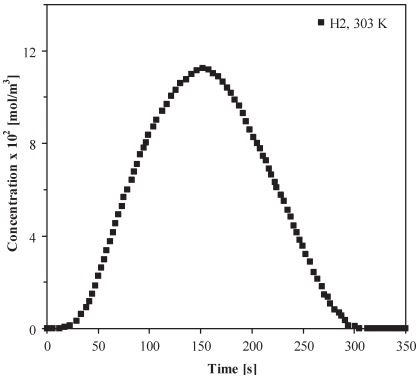

Figure 6. Pulse experiments of hydrogen on activated carbon at 303 (■); 1 bar of total pressure; experimental conditions are detailed in Table 2.

According to the full set of experiments it was determined that micropore resistances control diffusion for all the gases studied. At 303 K, the faster species is CO_2 while diffusion of CO is faster at higher temperatures. This indicates that the activation energy of diffusion is higher for CO (12.08 kJ/mol) than for CO_2 (9.75 kJ/mol). For CH_4, the larger molecule in this system, the energy of activation of micropore diffusion is 25.52 kJ/mol. This order does follow the expected order according to the size of the molecules (CO_2 > CO > CH_4). Diffusion of hydrogen was very fast in this material. In fact, its measurement is very difficult and the value reported in Table 6 is indicative of the order of magnitude of the micropore diffusion coefficient: in Equation (11) almost 80% of the resistance was in the axial dispersion term, being only 20% the resistance within the micropores.

Table 3. Diluted breakthrough experimental results obtained for CO_2 in activated carbon at 303, 323 and 343 K

Gas: CO_2	303 K	323 K	343 K
Flow rate [m^3/s]	6.25×10^{-7}	6.25×10^{-7}	6.25×10^{-7}
μ [s]	2852	1570	1118
σ^2[s]	182133	59289	33191
D_{ax}[m^2/s]	4.03×10^{-5}	4.27×10^{-5}	4.51×10^{-5}
D_m[m^2/s]	5.98×10^{-5}	6.66×10^{-5}	7.37×10^{-5}
D_k[m^2/s]	2.97×10^{-4}	3.07×10^{-4}	3.17×10^{-4}
D_p[m^2/s]	2.49×10^{-5}	2.74×10^{-5}	2.99×10^{-5}
k_f [m/s]	0.1184	0.1184	0.1184
D_c/r_c^2 [s^{-1}]	1.60×10^{-2}	2.30×10^{-2}	2.50×10^{-2}

Table 4. Pulse experimental results obtained for CH_4 in activated carbon at 303, 323 and 343 K

Gas: CH_4	303 K	323 K	343 K
Flow rate [m^3/s]	6.25×10^{-7}	6.25×10^{-7}	6.25×10^{-7}
μ [s]	903.4	528.0	322.9
σ^2[s]	52792	16596	6030
D_{ax}[m^2/s]	4.37×10^{-5}	4.64×10^{-5}	4.93×10^{-5}
D_m[m^2/s]	6.96×10^{-5}	7.74×10^{-5}	8.56×10^{-5}
D_k[m^2/s]	4.94×10^{-4}	5.10×10^{-4}	5.25×10^{-4}
D_p[m^2/s]	3.05×10^{-5}	3.36×10^{-5}	3.68×10^{-5}
k_f [m/s]	0.1184	0.1184	0.1184
D_c/r_c^2 [s^{-1}]	5.81×10^{-3}	1.13×10^{-2}	1.89×10^{-2}

Multicomponent Breakthrough Curves

In a PSA unit, the multicomponent mixture is fed to a set of columns operating according to a pre-defined scheduling. Thus, the modelling of fixed-bed behavior of the multicomponent mixture in a fixed-bed is essential to define a PSA unit. Initially we have performed a breakthrough curve of a H_2/CO_2 mixture and then the ternary $H_2/CO_2/CH_4$ mixture was employed. The operating conditions at which those experiments were performed are shown in Table 7.

The experimental results of the H_2/CO_2 binary mixture for two different temperatures (323 and 343 K) are detailed in Fig. 7. The bed was initially filled with helium and a very fast breakthrough of hydrogen can be observed according to the simulations. The typical roll-up of a weak adsorbed compound displaced by a more strongly adsorbed species was observed for hydrogen. The adsorption of CO_2 is accompanied with a

Table 5. Pulse experimental results obtained for CO in activated carbon at 303, 323 and 343 K

Gas: CO	303 K	323 K	343 K
Flow rate [m^3/s]	5.80×10^{-7}	5.80×10^{-7}	5.80×10^{-7}
μ [s]	185.3	122.0	87.02
σ^2 [s]	1687.6	681. 9	396.4
D_{ax}[m^2/s]	3.79×10^{-5}	4.17×10^{-5}	4.56×10^{-5}
D_m[m^2/s]	7.30×10^{-5}	8.12×10^{-5}	8.96×10^{-5}
D_k[m^2/s]	3.73×10^{-4}	3.85×10^{-4}	3.97×10^{-4}
D_p[m^2/s]	3.05×10^{-5}	3.35×10^{-5}	3.66×10^{-5}
k_f [m/s]	0.1184	0.1184	0.1184
D_c/r_c^2 [s^{-1}]	5.18×10^{-2}	8.18×10^{-2}	9.00×10^{-2}

Table 6. Pulse experimental results obtained for H_2 in activated carbon at 303 K

Gas: H_2	303 K
Flow rate [m^3/s]	1.167×10^{-6}
μ [s]	152.2
σ^2[s]	2962.3
D_{ax}[m^2/s]	6.18×10^{-5}
D_m[m^2/s]	1.61×10^{-4}
D_k[m^2/s]	1.40×10^{-3}
D_p[m^2/s]	2.40×10^{-5}
k_f [m/s]	0.1184
D_c/r_c^2 [s^{-1}]	5.05×10^{-2}

marked increase in temperature inside the column. Note that the experimental value measured at z = 0.68 m corresponds to the temperature of the column wall. The prediction of the mathematical model employing information obtained from pure component data of adsorption equilibrium and kinetics is also shown in Fig. 7 (solid lines). The transport parameters values used in the simulations are given in Table 8. A good agreement was observed between the experimental data and the predicted concentration history at the end of the column. The temperature evolution within the column was also well predicted. As mentioned before the thermocouple placed at z = 0.68 m from feed inlet is close to the column wall. For this reason, the prediction of the column wall temperature is also shown and it can be observed that the experimental data is close to the prediction of the column wall temperature

Table 7. Conditions used in binary (H_2/CO_2) and ternary ($H_2/CO_2/CH_4$) breakthrough experiments done with the activated carbon

Breakthrough experiments	Binary exp. I	Binary exp. II	Ternary exp. I
Column length [m]	0.87	0.87	0.87
Column diameter [m]	0.021	0.021	0.021
Mass of adsorbent [kg]	0.1760	0.1760	0.1743
Temperature [K]	323	343	305
Pressure [bar]	2.5	2.5	2.5
Mixture flow rate [m^3/s]	15.96×10^{-6}	15.96×10^{-6}	15.84×10^{-6}
Mixture molar fraction	CO_2: 0.176 H_2: 0.824	CO_2: 0.176 H_2: 0.824	CO_2: 0.159 H_2:0.795 CH_4: 0.046
N_2 flow rate [m^3/s]	75.30×10^{-6}	75.30×10^{-6}	75.30×10^{-6}
C_2H_6 flow rate [m^3/s]	0.30×10^{-6}	0.30×10^{-6}	—

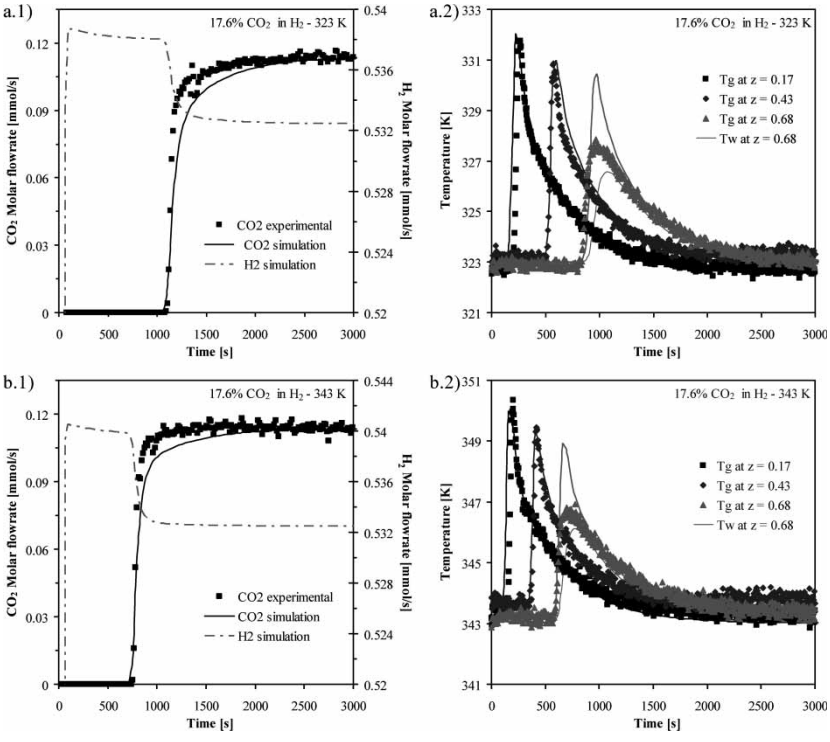

Figure 7. Binary H_2-CO_2 breakthrough results (points – experimental; lines – simulation): a) 323 K experience, b) 343 K experience; 1) CO_2 and H_2 molar flow rate profiles, 2) temperature profiles at 0.17, 0.43, 0.68 m from the bed inlet and the wall temperature Tw at 0.68 m from the bed inlet.

Table 8. Parameters values used in the simulations of the fixed bed experiments

Breakthrough experiments	Binary exp. I	Binary exp. II	Ternary exp. I
D_p [m^2/s][a]	CO_2: 4.48×10^{-6} H_2: 4.80×10^{-6}	CO_2: 4.94×10^{-6} H_2: 5.32×10^{-6}	CO_2: 3.57×10^{-6} H_2: 4.47×10^{-6} CH_4: 3.10×10^{-6}
D_m/r_m^2 [s^{-1}]	CO_2: 4.90×10^{-4} H_2: 5.05×10^{-2}	CO_2: 6.70×10^{-4} H_2: 5.05×10^{-2}	CO_2: 4.20×10^{-4} H_2: 5.05×10^{-2} CH_4: 9.48×10^{-5}
k_f [m/s]	3.98×10^{-2}	4.36×10^{-2}	3.19×10^{-2}
h_f [W/m^2K]	164	169	154
h_w [W/m^2K]	66.7	69.6	62.0
U [W/m^2K]	31.3	33.6	30.25

[a]values at inlet conditions

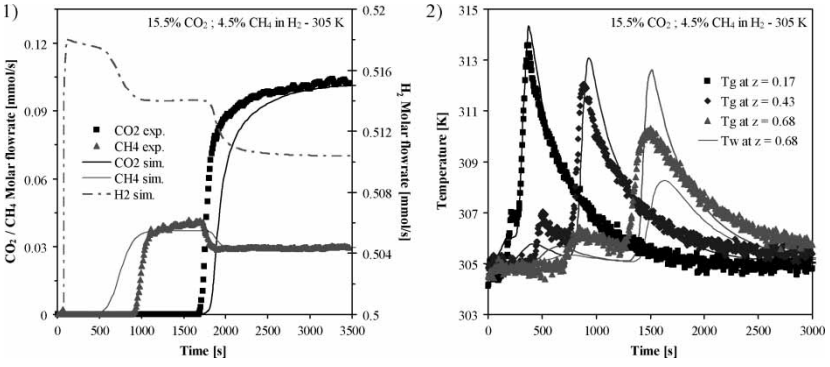

Figure 8. Ternary H_2-CO_2-CH_4 breakthrough results (points – experimental; lines – simulation): 1) CO_2,CH_4 and H_2 molar flow rate profiles, 2) temperature profiles at 0.17, 0.43, 0.68 m from the bed inlet and the wall temperature Tw at 0.68 m from the bed inlet.

but may be have some influence of the gas temperature, reason why the experimental value lays between these two values.

The experimental results of the ternary $H_2/CO_2/CH_4$ mixture are reported in Fig. 8. The experimental total flow rate history obtained for the ternary H_2-CO_2-CH_4breakthrough curve is shown in Fig. 9. In this case, hydrogen as the less adsorbed species pass through two plateaus until reaching the feed concentration, once the column is in equilibrium with all the adsorbates. The roll-up is also observed by methane being displaced by CO_2, which is strongly adsorbed. The temperature profiles within the column can also be very well defined, particularly at the end of the column where an initial increase in temperature due to methane adsorption can be

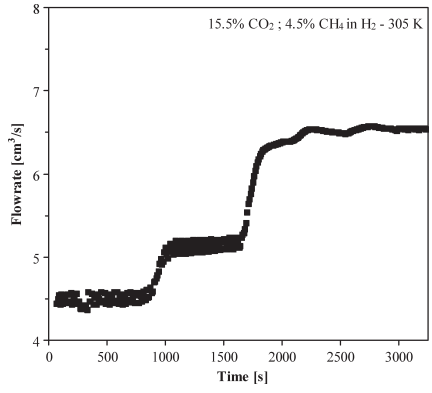

Figure 9. Total flow rate at the column outlet obtained for the ternary H_2-CO_2-CH_4 breakthrough curve on activated carbon.

observed followed by a stronger peak of CO_2 adsorption. In this experiment, there was a deviation lower than 10% between the adsorbed amount obtained experimentally and the predicted by the mathematical model. This may be due to two possible and different reasons. The first one is that a small experimental error in the determination of methane is very important because of the low molar fraction employed in the experiment. The second possibility is that the capacity of methane predicted by the multicomponent extension of the Virial model is smaller at low partial pressures. As the model predicts a lower adsorption capacity for methane, its simulated concentration front reaches the end of the column sooner than the experimental. It should be mentioned that the model used to predict multicomponent data is based on parameters estimated from pure component isotherms. Also, the estimation of Virial coefficients A_{ij} and B_{ijk} was done by a simple arithmetic average obtained from Amagat's rule instead of a geometric average (20).The disagreement in the adsorption capacity is also reflected as a time-deviation and intensity in the prediction of the temperature histories in the column. In agreement with the experimental results, two different temperature increases are observed: the first one due to methane and the second because of CO_2 adsorption.

According to the experimental results observed it was shown that the activated carbon employed can be used for selective removal of CO_2 and CH_4 in off-gases of methane steam reforming (7). The possibility of removal of CO and N_2 in this adsorbent can also be evaluated.

CONCLUSIONS

Adsorption equilibrium and kinetics of five different pure gases (H_2, CO_2, CH_4, CO, and N_2) were evaluated in a commercial sample of activated carbon to be employed in Pressure Swing Adsorption (PSA) unit for hydrogen purification. Adsorption properties were measured at 303, 323, and 343 K in a pressure range between 0–22 bar. The isotherms were fitted with the Virial isotherm model that has direct theoretical extension for the prediction of multicomponent behavior. This model showed great flexibility to fit the complete set of adsorption equilibrium data of the different gases. Adsorption kinetics of the pure gases was also measured and in all cases the diffusion was controlled within the micropore structure of the activated carbon. Diffusion of H_2 was very fast and hard to measure by any macroscopic technique.

Binary (H_2-CO_2) and ternary (H_2-CO_2-CH_4) breakthrough curves were measured and simulated to validate the predictions of a mathematical model for a fixed bed based on parameters measured for pure components. It was observed that for low concentrations of methane, the amount adsorbed predicted by the multicomponent extension of the Virial isotherm is slightly different from the experimental value.

The experimental and simulation results show that the activated carbon employed in this study can be used in a PSA unit to selectively remove CO_2 and CH_4 to produce high purity hydrogen stream and also delivering H_2 -free CO_2 stream directly for sequestration, as required by new clean technologies to produce fuels and energy.

NOMENCLATURE

a_p	particle specific area ($m^2 \cdot kg$)
A	Virial coefficients (m^2/mol)
B	Virial coefficients (m^4/mol^2)
Bi_i	mass Biot number of component i
c	concentration (mol/kg)
$c_{g,i}$	component i gas phase concentration (mol/kg)
$c_{g,T}$	total gas phase concentration (mol/kg)
C_p	gas mixture molar specific heat at constant pressure ($J/mol \cdot K$)
$\overline{C_{m,i}}$	average concentration of component i in the macropores (mol/m^3)
$\hat{C}_{p,s}$	particle specific heat at constant pressure [per mass unit] ($J/kg \cdot K$)
$\overline{C_{m,T}}$	average total concentration in the macropores (mol/m^3)
$\hat{C}_{p,w}$	wall specific heat at constant pressure [per mass unit] ($J/kg \cdot K$)
$C_{s,i}$	component i concentration at the solid surface (mol/kg)
C_v	gas mixture molar specific heat at constant volume ($J/mol \cdot K$)
$C_{v,i}$	molar specific heat of component i at constant volume ($J/mol \cdot K$)
$C_{v,ads,i}$	molar specific heat of component i in the adsorbed phase at constant volume ($J/mol \cdot K$)
d_p	particle diameter (m)
d_{we}	wall external diameter (m)
d_{wi}	wall internal diameter (m)
D_{ax}	axial dispersion coefficient (m^2/s)
D_c	micropore diffusivity (m^2/s)
D_c^0	limiting diffusivity at infinite temperatures (m^2/s)
D_{ij}	binary molecular diffusivity (m^2/s)
D_m	molecular diffusivity (m^2/s)
D_p	macropore diffusivity (m^2/s)
D_k	Knudsen diffusivity (m^2/s)
e	wall thickness (m)
E_a	activation energy of micropore diffusion (kJ/mol)
ERR	error function (%)
g	acceleration due to gravity (m/s^2)
Gr	Grashof number
h_{ex}	external convective heat transfer coefficient ($J/s \cdot m^2 \cdot K$)

h_f	film heat transfer coefficient between the gas phase and the particle ($J/s \cdot m^2 \cdot K$)
h_w	film heat transfer coefficient between the gas phase and the wall ($J/s \cdot m^2 \cdot K$)
k_f	film mass transfer coefficient (m/s)
k_g	gas conductivity ($J/s \cdot m \cdot K$)
K_H	Henry constant ($mol/kg \cdot bar$)
K_∞	adsorption constant at infinite temperature ($mol/kg \cdot bar$)
L	column length (m)
m_{ads}	mass of adsorbed gas (kg)
m_s	mass of adsorbent (kg)
M_W	molecular weight of the gas (kg/mol)
N	number of points of each isotherm
Nu	Nusselt number
P	pressure (Pa)
Pr	Prandt number
q	absolute adsorbed phase concentration (mol/kg)
q_{cal}	calculated adsorbed phase concentration (mol/kg)
$q_{\exp}$	experimental adsorbed phase concentration (mol/kg)
$\bar{q}_i$	particle averaged adsorbed concentration (mol/kg)
q_i^*	adsorbed concentration in equilibrium with $\overline{C_{m,i}}$ (mol/kg)
r_c	"microparticle" radius (m)
r_p	mean pore radius (m)
R_g	universal gas constant ($J/mol \cdot K$)
R_p	radius of the adsorbent extrudate (m)
Ra	Rayleigh number
Re	Reynolds number
S	adsorbent specific area ($m^2 \cdot kg$)
Sc	Schmidt number
Sh	Sherwood number
t	time (s)
T	temperature (K)
T_{film}	film temperature (K)
T_g	gas temperature (K)
T_p	particle temperature (K)
T_w	wall temperature (K)
T_∞	external temperature (K)
u_0	superficial velocity (m/s)
u_i	interstitial velocity (m/s)
U	overall heat transfer coefficient ($J/s \cdot m^2 \cdot K$)
V_{ads}	volume of adsorbent (m^3)
V_c	volume of the cell where the adsorbent is located (m^3)
V_s	volume of the solid adsorbent (m^3)
w	weight SOR-ARE parameter, $0 \leq w \leq 1$

y_i	molar fraction of component i
z	axial position

NOTATION

Greek Letters

α	external thermal diffusivity ($W/m \cdot K$)
α_w	ratio of the internal surface area to the volume of the column wall (m^{-1})
$\alpha_{w\ell}$	ratio of the logarithmic mean surface area of the column shell to the volume of the column wall (m^{-1})
β	thermal expansion coefficient ($m/m \cdot K$)
Δm	difference of weight between two measurements (kg)
$(-\Delta H)$	isosteric heat of adsorption (kJ/mol)
ε	bed porosity
ε_p	particle porosity
λ	heat axial dispersion coefficient ($J/s \cdot m \cdot K$)
λ_w	wall conductivity ($J/s \cdot m \cdot K$)
μ	gas viscosity ($Pa \cdot s$)
μ_1	first moment (s)
ν	kinematic viscosity of the external gas (m^2/s)
ρ_b	bulk density of the bed (kg/m^3)
ρ_g	density of the gas phase (kg/m^3)
ρ_ℓ	density of the adsorbed phase (kg/m^3)
ρ_p	adsorbent (particle) density (kg/m^3)
ρ_w	wall density (kg/m^3)
σ^2	second moment (s^2)
τ_p	pore tortuosity
Ω_c	geometric LDF factor for micro particles
Ω_m	geometric LDF factor for macro particles

ACKNOWLEDGMENT

The authors would like to thank financial support from European Project HY2SEPS (Hybrid Hydrogen – Carbon Dioxide Separation Systems), contract No 019887.

REFERENCES

1. CO_2 Capture and Storage. VGB Report on the State of the Art (2004). Available at: http://www.vgb.org/data/vgborg_/Fachgremien/Umwltschtz/VGB%20Capture%20and%20Storage.pdf.

2. Gale, J., Bachu, S., Bolland, O., and Xue, Z. (2007) To store or not to store? *International Journal Greenhouse Gas Control*, 1: 1.
3. European Research Project HY2SEPS (Hybrid Hydrogen Carbon Dioxide Separation Processes) website http://hy2seps.iceht.forth.gr/.
4. Yang, J. and Lee, C.-H. (1998) Adsorption dynamics of layered bed PSA for H2 recovery from coke oven gas. *AIChE Journal*, 44: 1325.
5. Ahn, H., Lee, C.-H., Seo, B., Yang, J., and Baek, K. (1999) Backfill cycle of layered bed H2 PSA Process. *Adsorption*, 5: 419.
6. Sircar, S., Waldron, W., Rao, M.B., and Anand, M. (1999) Hydrogen production by hybrid SMR-PSA-SSF membrane system. *Separation and Purification Technology.*, 17: 11.
7. Sircar, S. and Golden, T.C. (2000) Purification of hydrogen by pressure swing adsorption. *Separation Science and Technology*, 35: 667.
8. Esteves, I.A.A.C. and Mota, J.P.B. (2002) Simulation of a new hybrid membrane/pressure swing adsorption process for gas separation. *Desalination*, 148: 275.
9. Zhou, L., Lü, C.-Z., Bian, S.-J., and Zhou, Y.-P. (2002) Pure hydrogen from dry gas refineries via a novel pressure swing adsorption process. *Industrial & Engineering Chemistry Research*, 41: 5290.
10. Jee, J.-G., Kim, M.-B., and Lee, C.-H. (2001) Adsorption characteristics of hydrogen mixtures in a layered bed: binary, ternary and five component mixtures. *Industrial & Engineering Chemistry Research*, 40: 868.
11. Murata, K. and Kaneko, K. (2000) Nano-range interfacial layer upon high-pressure adsorption of supercritical gases. *Chemical Physics Letters*, 321: 342.
12. Murata, K., Miyawaki, J., and Kaneko, K. (2002) A simple determination method of the absolute adsorbed amount for high pressure gas adsorption. *Carbon*, 40: 425.
13. Dreisbach, F., Staudt, R., and Keller, J.U. (1999) High pressure adsorption data of methane, nitrogen, carbon dioxide and their binary and ternary mixtures on activated carbon. *Adsorption*, 5: 215.
14. Cavenati, S. (2005) Adsorptive processes for separation of $CH_4/CO_2/N_2$ mixtures. Ph.D. Dissertation, University of Porto: Portugal.
15. Span, R. and Wagner, W. (1996) A new equation of state for carbon dioxide covering the fluid region from the triple-point temperature to 1100 K at pressures up to 800 MPa. *Journal of Physical and Chemical Reference Data*, 25: 1509.
16. Weast, R.C. (1973) *Handbook of Chemistry and Physics, a Ready-Reference Book of Chemical and Physical Data*, 54th Edn, The Chemical Rubber Co.
17. Do, D.D. (1998) Adsorption analysis: equilibria and kinetics. *Series on Chemical Engineering*; Vol. 2, Imperial College Press.
18. Kiselev, A.V. (1971) Vapor adsorption on zeolites considered as crystalline species adsorbents. *Molecular Sieve Zeolites-II, ACS series*, 102: 37.
19. Barrer, R.M. (1981) Sorption in porous crystals: equilibria and their interpretation. *Journal of Chemical Technology and Biotechnology*, 31: 71.
20. Taqvi, S.M. and LeVan, M.D. (1997) Virial Description of two-component adsorption on homogeneous and heterogeneous surfaces. *Industrial & Engineering Chemistry Research*, 36: 2197.
21. Prausnitz, J.M., Lichtenthaler, R.N., and De Azevedo, E.G. (1996) *Molecular Thermodynamics of Fluid-Phase Equilibria*; Prentice Hall: Englewood Cliffs, NJ.
22. Malek, A. and Farooq, S. (1996) Comparison of isotherm models for hydrocarbon adsorption on activated carbon. *AIChE Journal*, 42: 3191.
23. Ruthven, D.M. (1984) *Principal of Adsorption and Adsorption Processes*; John Wiley & Sons: New York.

24. Bird, R.B., Stewart, W.E., and Lightfoot, E.N. (2002) *Transport Phenomena*, 2nd Edn; Wiley International: Singapore.
25. Wakao, N. and Funazkri, T. (1978) Effect of fluid dispersion coefficients on particle-to-fluid mass transfer coeficients in packed beds. *Chemical Engineering Science*, 33: 1375.
26. Yang, R.T. (1987) *Gas Separation by Adsorption Processes*; Butterworths: Boston.
27. Incropera, F.P. and Witt, D.P. D. (1996) *Fundamentals of Heat and Mass Transfer*, 4th Edn; John Wiley & Sons: New York.
28. Wasch, A.P. D. and Froment, G.F. (1972) Heat transfer in packed beds. *Chemical Engineering Science*, 27: 567.
29. Da Silva, F.A., Silva, J.A., and Rodrigues, A.E. (1999) A general package for the simulation of cyclic adsorption processes. *Adsorption*, 5: 229.
30. Grande, C.A. and Rodrigues, A.E. (2005) Propane/propylene separation by pressure swing adsorption using zeolite 4A. *Industrial & Engineering Chemistry Research*, 44: 8815.
31. Cavenati, S., Grande, C.A., and Rodrigues, A.E. (2006) Separation of $CH_4/CO_2/N_2$ mixtures by layered pressure swing adsorption for upgrade of natural gas. *Chemical Engineering Science*, 61: 3893.
32. Siriwardane, R.V., Shen, M.-S., Fisher, E.P., and Poston, J.A. (2001) Adsorption of CO_2 on molecular sieves and activated carbon. *Energy & Fuels*, 15: 279.
33. Siriwardane, R.V., Shen, M.-S., Fisher, E.P., Poston, J.A., and Shamsi, A. (2001) Adsorption and desorption of CO_2 on solid sorbents, U.S. Department of Energy, NETL Publications, (Conference Proceedings on Carbon Sequestration - First National Conference on Carbon Sequestration, Session 3B. Capture & Sequestration III: Adsorption Studies).
34. Siriwardane, R.V., Shen, M.-S., and Fisher, E.P. (2005) Adsorption of CO_2 on zeolites at moderate temperature. *Energy & Fuels*, 19: 1153.
35. Jayaraman, A., Chiao, A.S., Padin, J., Yang, R.T., and Munson, C.L. (2002) Kinetic separation of methane/carbon dioxide by molecular sieve carbons. *Separation Science and Technology*, 37: 2505.
36. Marathe, R.P., Mantri, K., Srinivasan, M.P., and Farooq, S. (2004) Effect of ion exchange and dehydration temperature on the adsorption and diffusion of gases in ETS-4. *Industrial & Engineering Chemistry Research*, 43: 5281.
37. Eic, M. and Ruthven, D.M. (1988) New experimental technique for measurement of intracrystalline diffusivity. *Zeolites*, 8: 40.
38. Grande, C.A. and Rodrigues, A.E. (2004) Adsorption kinetics of propane and propylene in zeolite 4A. *Chemical Engineering Research and Design*, 82: 1604.
39. Glover, C.J. and Lau, W.R. (1983) Determination of multicomponent sorption equilibria using perturbation gas chromatography. *AIChE Journal*, 29: 73.